Mario Caruso, Emanuela Gatto, Antonio Palleschi, Manuela Scarselli, Maurizio De Crescenzi, Fernando Formaggio, Edoardo Longo, Claudio Toniolo, Karen Wright, and Mariano Venanzi*

Are Two Better Than One? A New Approach for Multidentate Grafting of Peptides to a Gold Substrate

DOI 10.1515/zpch-2015-0729
Received November 5, 2015; accepted April 9, 2016

Abstract: Multidentate binding of two helical hexapeptides to a gold surface was obtained by introducing in the peptide chain a non ribosomial amino acid, i.e. the 4-amino-1,2-dithiolane-4-carboxylic acid (Adt) residue, a C^{α}-tetrasubstituted α-amino acid bearing a heterocyclic side chain characterized by a disulfide group. The two peptides, mainly formed by strongly helicogenic C^{α}-tetrasubstituted α-amino acids, were both functionalized at the N-terminus by a ferrocenoyl (Fc) group, but differ in the number of Adt residues included in the peptide chain: the former (Fc6Adt2) contains two Adt residues at positions 1 and 4, while its analog (Fc6Adt1) contains a single Adt at position 4, since the Adt at position 1 is substituted by an α-amino isobutyric acid (Aib) residue. This peptide design allowed us to explore the different electrochemical properties and morphologies shown by the two peptide layers immobilized on a gold surface by two (Fc6Adt2) or a single (Fc6Adt1) bidentate linker, respectively. The electrochemical activity of the ferrocenoyl probe embedded in the peptide film was characterized by cyclic voltammetry, chronoamperometry and square wave voltammetry, while the binding and the morphology of the peptide layers were studied by X-ray photoelectron

***Corresponding author: Mariano Venanzi,** Department of Chemical Sciences and Technologies, University of Rome 'Tor Vergata', 00133 Rome, Italy, e-mail: venanzi@uniroma2.it
Mario Caruso, Emanuela Gatto, Antonio Palleschi: Department of Chemical Sciences and Technologies, University of Rome 'Tor Vergata', 00133 Rome, Italy
Manuela Scarselli, Maurizio De Crescenzi: Department of Physics, University of Rome 'Tor Vergata', 00133 Rome, Italy
Fernando Formaggio, Edoardo Longo, Claudio Toniolo: ICB, Padova Unit, CNR, Department of Chemistry, University of Padova, 35131 Padova, Italy
Karen Wright: Institute Lavoisier de Versailles, UMR 8180, University of Versailles, 78035 Versailles, France

spectroscopy (XPS) and ultra high vacuum scanning tunneling microscopy (UHV-STM), respectively. Significant differences were observed in the electron transfer (ET) properties of the two peptides investigated, which emerge from the diverging morphology achieved by the peptide layers on the gold surface. It was found that while a standing-up configuration of the peptide layer, realized by a single bidentate linkage, maximizes the ET efficiency, a lying down configuration (two Adt linkages) allows for precise positioning of Fc in the proximity of a gold surface.

Keywords: 4-Amino-1,2-dithiolane-4-carboxylic acid (Adt), Ferrocenoyl-Peptide Conjugates, Peptide Foldamers, Peptide Materials, Peptide Self-Assembled Monolayers.

1 Introduction

The covalent linkage of self-assembled monolayers (SAMs) is the most successful approach for a stable functionalization of metal surfaces with organic layers [1]. Densely-packed films can be prepared to engineer surfaces with nanoscale precision, leading to a variety of applications from biosensing [2] to drug delivery [3], anti-adhesive low-fouling coating [4], and molecular electronics [5]. Most of the research activity so far concerned alkanethiol SAMs, but recently peptide-based SAMs have been gaining increasing attention for their unique properties and specific advantages for bio-inspired nanotechnology [6].

Unfortunately, alkanethiolate monolayers have been found to degrade with time and readily desorb upon heating [7]. A possible strategy to increase the stability of thiol-capped SAM is multidentate binding using di- or tri-sulfide linkers [8]. Kim et al. [9] used *o*-xylene-$\alpha\alpha'$-dithiol to form a close-packed, highly ordered monolayer on gold. They showed that the two sulfur atoms of the dithiol group were spanning a distance of 5 Å with no torsional strain, making double linking to Au(111) surface possible. However, the exact location of the sulfur atoms on the gold lattice (hollow, top or bridge sites) has not yet been determined despite several experimental and computational investigations [10–12]. The involvement of gold adatoms (gold atoms lifted from the gold surface) in an Au-adatom-monothiolate (Au$\cdots$S) or Au-adatom-dithiolate (S$\cdots$Au$\cdots$S) configuration has recently been proposed [13, 14]. This still controversial situation is rather surprising in view of the fact that the very first paper introducing SAMs utilized a lipoic (disulfide) group for linking an alkanethiol chain to gold [15]. Recently, gold$\cdots$sulfur interaction at the nanoscale level has been extensively reviewed [16–18].

All of the alkanethiol or peptide layers so far investigated, almost exclusively concerned vertically arranged SAMs, in which interchain interactions concur to stabilize the organic film in an almost perpendicular orientation with respect to the gold surface.

Very recently, we proposed a new approach to obtain a peptide film in which the helical peptide building blocks would maintain a rigid, parallel orientation with respect to a gold surface [19]. The hexapeptide investigated, denoted in the following as Fc6Adt2, was functionalized at the N-terminus with a ferrocenoyl (Fc) group, a well-known electrochemical probe. Due to the predominant presence in the sequence of strongly helicogenic C^{α}-tetrasubstituted α-amino acids (4 out of 6), the peptide chain attained a 3_{10}-helix conformation, as confirmed by a 2D-NMR study in solution on Fc6Adt2 and an X-ray diffraction investigation in the crystal state for its precursor pentapeptide [19].

The peculiarity of this newly synthesized hexapeptide is that 2 out of the 6 residues were the non ribosomial 4-amino-1,2-dithiolane-4-carboxylic acid (Adt), a C^{α}-tetrasubstituted α-amino acid bearing a heterocyclic side chain characterized by a disulfide group (Scheme 1). Adt was first synthesized in the early 1970s as an organic building block [20], (its derivatives useful for peptide synthesis were reported much more recently [21]), and discovered after three decades in a few natural compounds (Kottamides A-E) produced by *Pycnoclavella kottae* [22].

Insertion of the two Adt residues at the first and fourth positions of Fc6Adt2, together with the threefold 3_{10}-helical arrangement of the peptide chain, allowed us to get the two disulfide groups properly oriented for achieving a simultaneous, bidentate linkage to the gold surface. In this spatial configuration, the helical hexapeptide would be rigidly held in a parallel orientation with respect to the gold surface. Interestingly, the ferrocenoyl probe maintained its fully reversible electrochemical activity despite its close proximity to the metal surface [19].

In this contribution, we compare the structural and dynamical properties of Fc6Adt2 with those of a hexapeptide analog, denoted as Fc6Adt1, in which the Adt at position 1 of Fc6Adt2 was replaced by an α-amino-isobutyric acid (Aib)

Fc-CO-Aib-L-Ala-Aib-Adt-L-Ala-Aib-OMe (Fc6Adt1)

Fc-CO-Adt-L-Ala-Aib-Adt-L-Ala-Aib-OMe (Fc6Adt2)

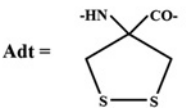

Scheme 1: Molecular structure and acronyms of the peptides investigated. The molecular structure of Adt is also shown.

residue (Scheme 1). As Aib is also a C^{α}-tetrasubstituted α-amino acid, we expect that the peptide secondary structure would not be perturbed by this substitution. However, in the case of Fc6Adt1 only a single bidentate Au$\cdots$S linkage can be formed. We will see later in the text how this single-point sequence mutation, will change the morphology of the peptide layer on the gold surface and will affect the electrochemical behavior of the Fc probe.

2 Experimental

2.1 Synthesis

4-amino-1,2-dithiolane-4-carboxylic acid was synthesized following the synthetic procedure reported as *Supplementary Information* (SI). Peptide synthesis was carried out using step-by-step methodologies in solution [23], i.e. Fmoc(fluorenyl-9-methyloxycarbonyl)-protection for the Adt residue and Boc (*tert*-butyloxycarbonyl) chemistry for the Aib and Ala residues. Fc-CO-Aib-OH and Fc-CO-AdtOH were prepared separately and successively conjugated to the pentapeptide precursor H-L-Ala-Aib-Adt-L-Ala-Aib-OMe (OMe, methoxy) to yield the final products Fc-CO-Aib-L-Ala-Aib-Adt-L-Ala-Aib-OMe (Fc6Adt1) and Fc-CO-(Adt-L-Ala-Aib)$_2$-OMe (Fc6Adt2), respectively. Details on the synthesis and characterization of Fc6Adt2 were already reported elsewhere [19], while the protocol for the synthesis of Fc6Adt1 was reported in the SI. Intermediate and final products were all characterized by FTIR absorption, ^{1}H- and ^{13}C NMR, and mass spectroscopy (SI).

2.2 Peptide-modified gold substrates

Gold foil electrodes were preliminarily etched in a piranha solution (2 : 1 sulfuric acid/H_2O_2, v/v) for 15 min and then rinsed with bidistilled water and ethanol. Peptide-coated electrodes were prepared by dipping the cleaned gold substrate for 18 h into a 1 mM chloroform solution of the peptides investigated under an Ar atmosphere. The peptide-modified electrodes were rinsed (5 times) with chloroform to remove physically adsorbed peptides, and dried for 3 min under an N_2 flow. For scanning tunneling microscopy (STM) experiments, ultraflat gold wafers were immersed overnight in a millimolar peptide ethanol solution, following the same deposition and rinsing procedures described above.

2.3 Fourier transform infrared absorption

FTIR absorption spectra in KBr disks were recorded on a Perkin-Elmer 580 B instrument equipped with PE-3600 data station. Spectra in $CDCl_3$ (98.8% Fluka) were recorded on a Perkin-Elmer 1720X instrument, using 0.1- and 1-cm CaF_2 cells. For each spectrum 50 scans at a resolution of 4 cm^{-1} were collected under an N_2 flow.

2.4 UV-Vis absorption

Absorption measurements were carried out on a Cary 100 SCAN (Varian, Palo Alto, CA) spectrophotometer. All experiments were carried out in quartz cells of variable optical length (0.1, 0.5, 1.0 cm).

2.5 Electronic Circular Dichroism (ECD)

ECD measurements were collected on a J-600 Jasco spectropolarimeter, using Hellma quartz cells (0.1-cm optical path length). Values are reported as total molar ellipticity (deg $\cdot$ cm^2 $\cdot$ $dmol^{-1}$): $[\Theta]_T = (MW \cdot \Theta)/(l \cdot c) = 3300 \times \Delta\varepsilon = 3300 \times (\varepsilon_L - \varepsilon_R)$, where Θ is the observed ellipticity, MW the molecular weight, l the optical path length (cm), c the peptide concentration (g/l), ε_L and ε_R are the molecular extinction coefficients under left- and right-handed circularly polarized light excitation, respectively.

2.6 X-ray photoelectron spectroscopy (XPS)

XPS data were acquired with a MAC2 (Riber Instruments, Rueil Mailmaison, France) semi-imaging analyzer, operating at a total energy resolution of 1.4 eV and using a non-monochromatized Al Kα (1486.6 eV) radiation source (14 kV, 300 W). Sample and anode were positioned at about 40 mm of distance, the illumination area was about $5 \cdot 5$ mm^2, and the take-off angle between the sample surface and the photoelectron energy analyzer was kept fixed at 45°. The energy scale was calibrated using the Au4f signal (84 eV with respect to the Fermi level) as reference. Energy distribution spectra were recorded over the Au4f, S2p, C1s, N1s and O1s photoelectron energy regions. XPS spectra were analyzed using a standard Gaussian curve fit routine with Shirley background subtraction [24], evaluating the quality of the fit by using the χ^2 minimization test. The widths of the Gaussian functions used for reproducing the experimental data, the energy dis-

tance and relative intensity of the components of the S2p states splitted by spin-orbit interaction were let free to vary in a restricted range during the fitting process.

2.7 Scanning tunneling microscopy measurements (STM)

STM experiments were carried out at room temperature under ultra-high vacuum conditions (4×10^{-10} mbar) using an Omicron-STM system (Omicron, Taunusstein, Germany). Electrochemically etched tungsten tips (99.9% purity, Goodfellow GmbH, Friedberg, Germany) were used. All images were acquired in the constant current mode and the collected data were not filtered apart from rigid plane subtraction.

2.8 Electrochemical methods

Cyclic voltammetry measurements were performed on a Heka PG310 potentiostat, by using a double junction calomel reference electrode, a *Pt* counter-electrode, and a gold thin foil, eventually modified by a chemisorbed peptide layer, as the working electrode. $NaClO_4$ 0.1 M in acetonitrile (20 ml) was used as a support electrolyte. The scan rate was varied from 50 to 300 mV s^{-1} at applied voltages comprised in the range from 0 to 0.9 V.

Chronoamperometry (CA) measurements were carried out with a PG-310 potentiostat in a standard three-electrode cell. The applied overpotential (η) was changed from negative (−0.3 V) to positive (+0.3 V) values with steps of 50 mV. The associated Tafel plots were fitted by linear regression analysis ($R \geq 0.98$).

Square wave voltammetry (SWV) experiments were carried out with an Autolab PGstat10 potentiostat in a standard three-electrode configuration. SWV experiments were recorded in the range between 0.2 V and 0.9 V, with a step potential of 0.01 V, amplitude of 0.025 V and frequencies in the range between 8 and 2000 Hz. The scan rate was 0.040 V/s.

2.9 Molecular mechanics (MM) calculations

MM calculations were carried out by using the MM4 force field [25, 26]. Initially, the peptides were assumed to adopt a 3_{10}-helix conformation using standard bond lengths and bond angles. Then, the conformational energy was optimized by taking into account electrostatic, non-bonding, hydrogen bond and torsional inter-

actions. Stretching and bending motions, as implemented in the MM4 force field, were also taken into account.

3 Results and discussion

3.1 Conformational studies in solution

As already stated above, the secondary structure of Fc6Adt2 was determined by 2D-NMR studies in solution, as well as by the X-ray diffraction structure of the pentapeptide precursor Boc-L-Ala-Aib-Adt-L-Ala-Aib [19]. Both peptides were found to populate preferentially a 3_{10}-helix conformation. In this section, we report on new spectroscopic data (FTIR absorption, CD) and MM calculations carried out to further characterize the conformational properties of the peptides investigated.

3.1.1 Fourier transform infrared absorption

The results of the FTIR absorption measurements on Fc6Adt1 and Fc6Adt2 in $CDCl_3$ were summarized in Table 1. The transitions occurring between 3200 and 3500 cm^{-1} (amide A) can be assigned to NH groups involved in H-bonds (below 3400 cm^{-1}) and 'free' NH groups (above 3400 cm^{-1}), respectively [27, 28]. Carbonyl stretching modes are usually observed between 1800 and 1500 cm^{-1} (~ 1730 cm^{-1} ester, ~ 1660 cm^{-1} amide I, ~ 1520 cm^{-1} amide II).

As reported in the literature [27–30], values of the amide I transition below 1660 cm^{-1} indicate the predominant population of an α-helical conformation, whereas values above 1660 cm^{-1} are typical of the preferred population of a 3_{10}-helix structure. As seen in Table 1, the very strong amide I transition for the hexapeptides investigated is located in the range 1668–1670 cm^{-1}, in good agreement with the values characteristic of a 3_{10}-helix. It should be noted that the FTIR absorption spectra in the amide A region, recorded in $CDCl_3$ at 10^{-3} M

Table 1: FTIR absorption bands for Fc6Adt2 and Fc6Adt1. All spectra were recorded in $CDCl_3$ at 10^{-3} M concentration. Underlined values refer to the strongest peaks.

Compound	IR absorption wavenumbers/cm^{-1}
Fc6Adt1	3691, 3607, 3431, 3327, 2989, 2934, 1734, <u>1668</u>, 1524
Fc6Adt2	3699, 3609, 3431, 3325, 2987, 2931, 1734, <u>1670</u>, 1524

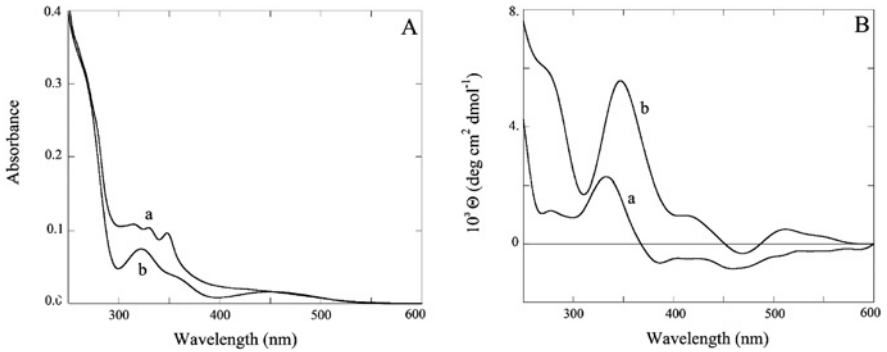

Figure 1: UV-Vis absorption (A) and ECD (B) spectra of Fc6Adt1 (a) and Fc6Adt2 (b). All of the spectra were measured for 10^{-4} M peptide solutions in $CDCl_3$, using a 1 cm cell length. ECD spectra were normalized with respect to the peptide molar concentration.

and 10^{-4} M peptide concentrations, are strictly overlapping which confirms the intramolecular nature of the H-bonded NH signals.

3.1.2 UV-Vis absorption and ECD

The amide groups and the Fc chromophore feature characteristic absorption bands in the near UV-Vis range. However, because of the extended overlap between the amide and Fc transitions, the wavelength region from 250 to 200 nm, the most useful for assessing the peptide conformation from ECD spectroscopy data, could be hardly informative. For this reason, only the ECD spectra of Fc6Adt1 and Fc6Adt2 ($CDCl_3$, 10^{-4} M) in the Vis region, safely ascribable to the Fc chromophore, were reported in Figure 1B, along with the corresponding absorption spectra (Figure 1A) recorded in the same region. Interestingly, a distinct ECD signal at 330–340 nm can be observed, as a result of the induced Cotton effect exerted by the chiral peptide chain on the covalently bound achiral Fc chromophore.

It should be noted that any induced chirality contribution can arise from neither Adt nor Aib, the nearest residue covalently bound to the Fc chromophore in Fc6Adt2 and Fc6Adt1, respectively. Therefore, the induced chirality on Fc can be assigned to an overall conformational asymmetry, which confirms the helical arrangement of the peptide chain. Furthermore, the ECD curves reported in Figure 1B show that the induced chirality effect is more intense for Fc6Adt2, indicating a more pronounced conformational bias for the latter peptide, i.e. that the Adt residue is more efficient than Aib in reducing the conformational heterogeneity of the N-terminal Fc probe.

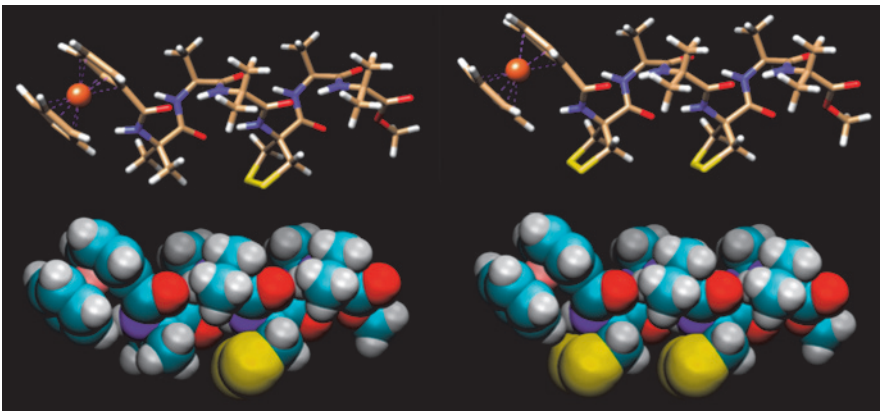

Figure 2: Ball-and-stick (top) and filled-sphere (bottom) representations of Fc6Adt1 (left) and Fc6Adt2 (right) from MM calculations. Light blue: carbon atoms; red: oxygen; blue: nitrogen; silver: hydrogen; yellow: sulfur.

3.1.3 Molecular Mechanics (MM)

Following the indications of the experimental results in solution and in the crystal state, we carried out MM calculations, initially assuming the peptide backbone in a 3_{10}-helix conformation. The total conformational energy of the peptide was therefore optimized, considering stretching and bending motions of both the peptide backbone and side-chains. The resulting minimum energy conformers for Fc6Adt1 and Fc6Adt2 were reported in Figure 2 in a ball-and-stick and a filled-sphere representations. This Figure clearly reveals the compact 3D-structure of the two peptides and the appropriate positioning of the Adt disulfide groups for interacting with the gold surface when the peptides attain a 3_{10}-helix conformation.

In summary, both experimental and computational results indicate that we have synthesized helical peptide building blocks of about 2-nm length, 0.6-nm width, and 1-nm height, prone to stable, multidentate binding to a gold surface.

3.2 Characterization of peptide layers on a gold surface

3.2.1 X-ray photoelectron spectroscopy (XPS)

XPS measurements were carried out to characterize the binding of Fc6Adt1 and Fc6Adt2 to the gold surface, and, in particular, to analyze the Au$\cdots$S interaction

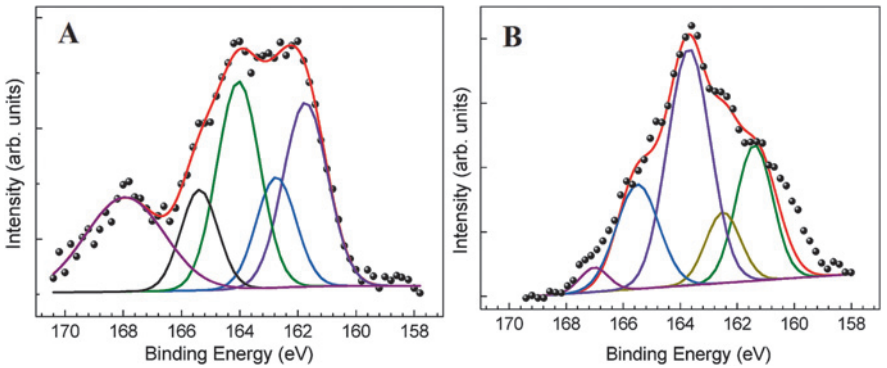

Figure 3: S2p XPS spectra of Fc6Adt1 (A) and Fc6Adt2 (B) on a gold surface. Filled circles: experimental points; red curve: fitting curve of the experimental data, obtained by the sum of Gaussian distributions (see Table 2 for assignment).

Table 2: Parameters of the Gaussian fitting functions used for reconstructing the XPS absorption bands of Fc6Adt2 and Fc6Adt1 in the S2p region.

Compound	Position (eV)	Intensity (a.u.)	Width (eV)	Assignment
Fc6Adt1	161.7	83.2	1.8	$S2p_{3/2}$
	162.7	50.0	1.6	$S2p_{1/2}$ (bonded)
	164.0	93.8	1.7	$S2p_{3/2}$
	165.4	45.5	1.5	$S2p_{1/2}$ (non or weakly bonded)
	167.9	42.6	3.2	Sulfoxides or sulfones
Fc6Adt2	161.4	211.4	1.5	$S2p_{3/2}$
	162.5	110.0	1.4	$S2p_{1/2}$ (bonded)
	163.7	367.6	1.8	$S2p_{3/2}$
	165.5	162.5	1.8	$S2p_{1/2}$ (non or weakly bonded)
	167.0	38.0	1.1	Sulfoxides or sulfones

established by the Adt side chains of the two peptides with the underlying gold lattice [31]. In Figure 3 and Table 2 the signals associated to the S2p orbitals of the dithiol groups in Fc6Adt1 and Fc6Adt2, both interacting with the gold surface, are reported. For the former compound, the low-energy doublet centered at 161.7 ($2p_{3/2}$) and 162.7 eV ($2p_{1/2}$) was assigned to S atoms (thiolates) strongly bonded

to the hollow sites of the gold lattice [32]. The energy difference (1 eV) and area ratio (1.9) of the doublet components are typical of 2p states splitted by spin-orbit interaction.

More problematic is the assignment of the doublet centered at 164.0 ($S2p_{3/2}$) and 165.4 eV ($S2p_{1/2}$). In the literature this signal was assigned to free SH groups [33], disulfide [34] or weakly bonded (adsorbed) S atoms on top of gold adatoms [13, 14], respectively.

In this case, the almost equal fraction (38%) of the two doublet signals strongly suggests that Fc6Adt1 predominantly attains a standing up configuration, with one of the S atoms chemisorbed on the Au surface (thiolate) and the other physisorbed on gold atoms. The broad absorption band at around 168 eV (23%) is typical of sulfoxides or sulfones [17].

Similar results have been obtained for the Adt S atoms in Fc6Adt2 (Figure 3B), either bonded to the Au hollow sites as thiolates (doublet at 161.4 and 162.5 eV), or weakly interacting with Au adatoms (doublet at 163.7 and 165.5 eV). In the latter case, the intensity ratio between the two predominant peaks at 161.4 and 163.7 eV indicates that mixed domains of lying down (1 : 1 bonded/weakly bonded S atoms) and standing up (1 : 3 bonded/weakly bonded S atoms) phases coexist. A minor component of oxidized sulfur atoms was also detected at around 167 eV.

However, it should be noted that a significant contribution from peptide multilayers (free disulfide), to the doublet at 163.7 and 165.5 eV cannot be excluded for both Fc6Adt1 and Fc6Adt2.

In summary, XPS data indicate that both peptides investigated are stably chemisorbed to the gold surface through Au···S linkages. However, while Fc6Adt1 predominantly attains a standing up configuration on the gold surface, Fc6Adt2 gives rise to both standing up and lying down domains, favored by the presence of two Adt disulfide clips.

3.2.2 Scanning tunneling microscopy (STM)

STM measurements provided important information on the morphology of the two peptide layers on the gold substrate. STM imaging under ultra-high vacuum conditions of the bare gold substrate shows wide atomically-flat terraces, separated by steps about 0.3-nm high, corresponding to the Au(111) monoatomic step (0.24 nm). Higher straight steps (2 to 5 atomic layers high) were also observed, probably produced by dislocations during the growth of the gold substrate.

STM imaging of Fc6Adt1 and Fc6Adt2 on gold revealed that extended regions of the Au surface are modified by the presence of peptide layers (SI). In

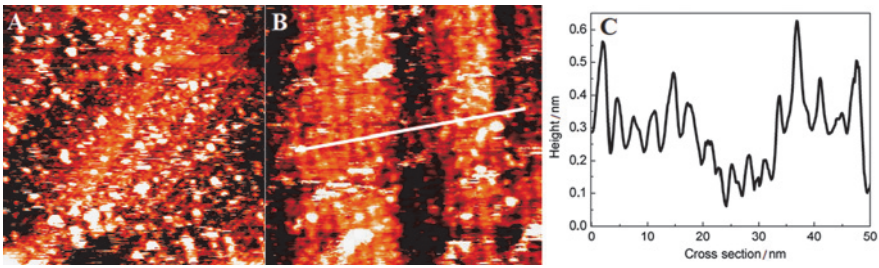

Figure 4: STM images of two different regions of the Fc6Adt2 film on gold, imaging a peptide multilayer region (A, $100 \times 100\ \mathrm{nm}^2$) and a stripe domain (B, $60 \times 60\ \mathrm{nm}^2$). Bright spots of 2 nm-width and 0.5 nm-height can also be seen in both images. C: height profile taken along the line drawn in Figure 4B (Tunneling conditions: $I = 300\ \mathrm{pA}$, $V = 1\ \mathrm{V}$).

the case of Fc6Adt2, large areas of the investigated surface domains showed ordered stripe-like structures (Figure 4). STM profiles of these domains (Figure 4C) revealed stripes 3-nm wide and 0.3-nm high, suggesting that these structures could be formed by bundles of peptides horizontally layered on the gold surface. A stripe-like morphology has already been found in alkanethiol-based monolayers obtained by vapor deposition [35], or solution deposition of short-chain alkanethiols [36]. Under these conditions, a low density of molecules on the surface is achieved, giving rise to regularly spaced structures with the alkyl chains parallel to the gold surface. Stripe structures were also observed by us in the case of a helical hexapeptide formed by C^{α}-tetrasubstituted α-amino acids and functionalized at the N-terminus by a lipoic group for covalent linking to gold [37].

Bright circularly-shaped nanometric spots were also seen in all the recorded STM images. A statistical analysis indicates that these bright structures feature average diameters of about 2.0 nm and heights of about 0.5 nm. These spots could be tentatively assigned to Fc groups protruding from the gold surface in small peptide clusters linked to the gold surface through the sole Adt^4 side chain.

No regular structures like stripe domains were imaged by STM experiments on Fc6Adt1/Au. In this case, only peptide clusters 2 nm-wide and heights varying from 0.5 to a maximum of 1.5 nm could be observed. The bright spots imaged in Figure 5A and 5B can be assigned to electron-rich Fc groups protruding from the gold surface. The height profiles reported in Figure 5C confirmed the heterogeneous character of the Fc6Adt1 layer, in which the single peptide chains adopt almost random orientations with respect to the gold surface, giving rise to standing-up peptide clusters of different heights.

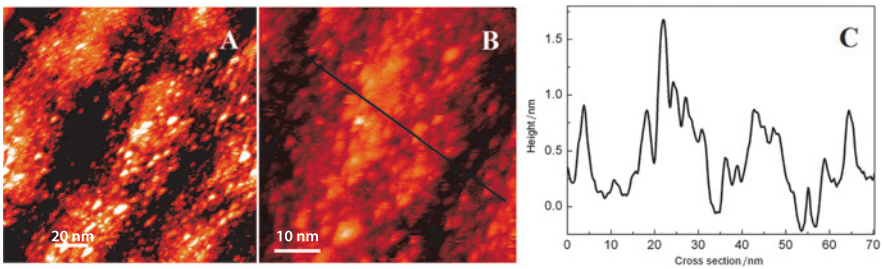

Figure 5: A and B: STM images of two different regions of the Fc6Adt1 film on gold, imaging a peptide multilayer region. C: Bright spots of 2 nm-width and variable heights (0.5–1.5 nm) can be seen in the image, the height profiles of which were taken along the line drawn in Figure 5B (Tunneling conditions: $I = 300$ pA, $V = 1$ V).

3.3 Electrochemical properties of the ferrocene-tagged peptide layer

3.3.1 Cyclic voltammetry (CV)

CV experiments were performed using a gold substrate modified by chemisorption of Fc6Adt1 or Fc6Adt2 as a working electrode in a three-electrode electrochemical cell, varying the applied potential from 0 to 0.9 V and the scan rate from 50 to 300 mV/s.

The typical reversible CV band of the Fc electroactive group ($E° = 0.55$ V vs. Ag/AgCl) was obtained for both compounds. In addition, it was found that the current intensity linearly increases with the scan rate of the CV experiments, which indicates that the Fc discharge is not affected by diffusive processes at the electrode/peptide interface, i.e. that both peptides are stably chemisorbed on the gold electrode (Figure 6). It should be noted that for a diffusion-limited process a dependence of the current intensity on the square root of the scan rate is generally observed [38].

Interestingly, the cathodic and anodic CV bands of both peptides are characterized by a larger full-width at half maximum (FWHM ≈ 150 mV) than it could be expected for a homogenous self-assembled monolayer (data not shown). Highly ordered SAMs generally show a low capacitive current, a zero peak splitting and a 90.6 mV half-width of the faradaic current peaks (for one exchanged electron). The broadening of the CV bands can be assigned either to thermodynamic or kinetic dispersion, i.e. a distribution of formal reduction potentials or rate constants, that could originate from self-interaction between Fc groups, heterogeneous binding of the peptide on the gold surface or defects of the peptide layer.

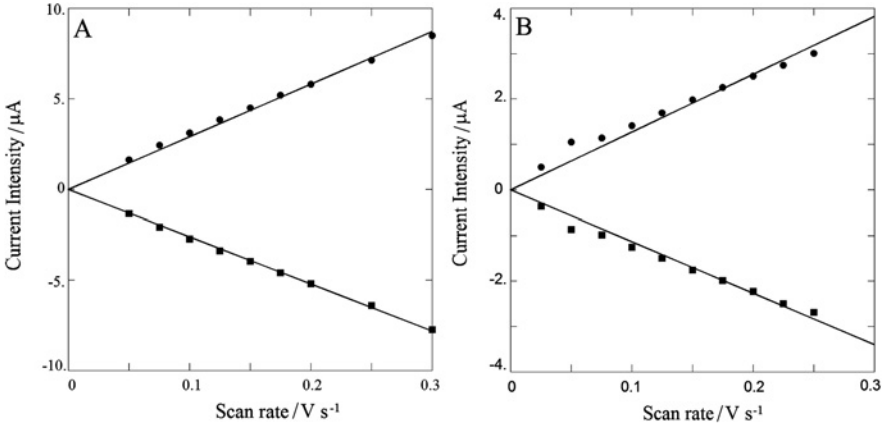

Figure 6: Cyclic voltammetry peak intensity current under cathodic (filled circles) and anodic (filled squares) conditions vs. scan rate for Fc6Adt1 (A) and Fc6Adt2 (B). Continuous lines are obtained from a least-squares linear fit of the experimental data with the constrain $I = 0$ at $V = 0$.

The amount of Fc6Adt1 and Fc6Adt2 chemisorbed on the gold surface, i.e. the surface coverage Γ, can be determined from the dependence of the peak current intensity (i_p) on the scan rate (υ) [38]:

$$i_p = \frac{n^2F^2}{4RT} A\Gamma\upsilon \tag{1}$$

where A is the effective area of the electrode, n the number of electrons transferred, F the Faraday constant, R the gas constants and T the temperature. From the results reported in Figure 6 the amount of Fc6Adt2 and Fc6Adt1 chemisorbed on the gold electrodes are estimated to be $(2 \pm 1)\cdot 10^{-11}$ and $(1.6 \pm 1)\cdot 10^{-10}$ mol/cm^2, respectively. The latter value is quite similar to the surface density obtained by us in the case of a helical octapeptide SAM, attaining a close hexagonal packing with a tilt angle of 40–50° with respect to the surface normal [39–41]. Considering Fc6Adt1 and Fc6Adt2 in a 3_{10}-helix conformation, the area covered by a single peptide molecule layered on the gold surface is about 2 nm^2 for both peptides investigated, leading to a theoretical full-coverage density of 8.3×10^{-11} mol/cm^2.

These findings corroborate our view that Fc6Adt2 is predominantly horizontally layered on the gold electrode surface, while Fc6Adt1 clustered in almost randomly oriented peptide bundles.

3.3.2 Chronoamperometry (CA)

CA experiments are more sensitive to kinetic heterogeneity than other electrochemical techniques [42]. To better characterize the ET process at the peptide/metal interface, we therefore carried out CA experiments using a working electrode modified by deposition of an Fc6Adt1 or an Fc6Adt2 layer. The time-dependent current intensity, $I(t)$, generated upon reduction or oxidation of the surface-confined electroactive species after application of a potential bias, is given by Equation (2):

$$I(t) = \sum_i k_{\mathrm{et},i} Q_i e^{-k_{\mathrm{et},i} t} \tag{2}$$

where $k_{\mathrm{et},i}$ is the ET rate constant associated to the i-th species and Q_i is the charge associated with the reduction (or oxidation) of the i-th redox species adsorbed on the electrode surface. In the case of an homogeneous film, the current intensity decay $I(t)$ is described by a monoexponential time decay, which indicates the presence of a single redox component in a quite homogeneous environment [43].

In our case, we found that the CA current decays of Fc6Adt2 are adequately reproduced by two exponential time components, in the following referred as k_{et1} and k_{et2}. The dependence of these rate constants (on a log scale) on the applied overpotential η, i.e. the difference between the applied potential and the formal redox potential of Fc, is reported in the Figure 7A and 7B (Tafel plots) for both anodic and cathodic conditions, respectively. The heterogeneity of the ET process revealed by CA experiments on Fc6Adt2 clearly justifies the observed broadening of the CV peaks.

The anodic ($k_{\mathrm{et,\,a}}$) and cathodic ($k_{\mathrm{et,\,c}}$) rate constants are related to the applied overpotential η by the equation [42]:

$$k_{a(c)} = k_0 \exp\left[\pm \alpha_{a(c)} \frac{nF}{RT} \eta \right] \tag{3}$$

where the plus (minus) sign applies to anodic (cathodic) conditions. Values of the electronic coupling parameter $\alpha_{a(c)}$ can vary between 0 and 1 (for pure metals they are around 0.5, which indicates that the activated complex is exactly halfway on the reaction coordinate connecting the reagent and product regions). k_0 represents the limit ET rate constant at $\eta = 0$, i.e. at $E = E°$. From the data reported in Figure 7A and Figure 7B, we obtained $k_{0,1} = 11.7 \pm 0.5\ \mathrm{s}^{-1}$ and $k_{0,2} = 1.0 \pm 0.2\ \mathrm{s}^{-1}$ for the two time components accounting for the Fc6Adt2 current decays under either anodic or cathodic conditions.

Interestingly, the Tafel plots reported in Figure 7 show a very weak dependence of the k's rate constants on η, i.e. relatively small values of the electronic

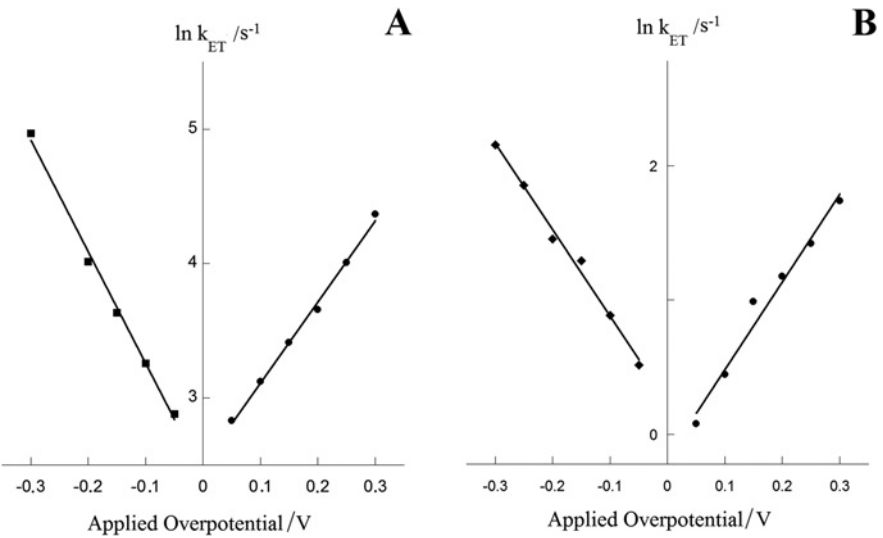

Figure 7: Dependence of the electron transfer rate constants (A: k_{et1}; B: k_{et2}) on the applied overpotential η (Tafel plot) under anodic ($\eta > 0$) and cathodic ($\eta < 0$) conditions for Fc6Adt2.

coupling parameter, with the same slope for both the current decay components under anodic and cathodic conditions ($\alpha_{a(c)} = 0.16 \pm 0.02$). From CA experiments, information on the amount of charge transferred from each species, i.e. Q_1 and Q_2 in Equation (2), can be extracted. We obtained $Q_1 \approx 2Q_2$, indicating that the faster process is able to transfer twice the charge exchanged through the slower process.

On the contrary, in the case of Fc6Adt1, CA experiments can be accounted for by a single exponential decay (actually, this rate constant should be considered as an average quantity due to the heterogeneity of the Fc6Adt1 layer). From the associated Tafel plot, the ET rate constants at $E = E°$ under anodic and cathodic conditions were found to be quite similar ($k_{0,a} = 12 \pm 2\ s^{-1}$, $k_{0,c} = 12 \pm 5\ s^{-1}$). Unfortunately, the relatively large standard deviations, most likely determined by the heterogeneity of the peptide layer, make not possible to assess the role of the peptide chain in the ET process.

From the slopes of the Tafel plots, we obtained even smaller values for the electronic coupling parameters of Fc6Adt1 ($\alpha_a = 0.04 \pm 0.03$, $\alpha_c = 0.03 \pm 0.02$). These results indicate that a substantially different Fc/Au coupling is realized by the two peptide layers.

The low values obtained for the electronic coupling parameter α are typical of ET driven by electron hopping through the amide sites. This mechanism is strongly favored by the alignment of the energy levels of the amide HOMO (−6.5 eV), the S atom HOMO (−5.5 eV), and the gold Fermi level (−5.1 eV) [44].

The high-energy level of the amide LUMO (−1.2 V) makes the competitive superexchange mechanism definitely less probable.

Summarizing the results of CA measurements on Fc6Adt1 and Fc6Adt2, we are tempted to assign the faster ET process ($k_0 \approx 11-12\ s^{-1}$) to Fc groups that transfer electrons through peptide chains attaining a standing-up configuration, i.e. linked to the gold surface by a single Adt residue.

The slow decay component measured for Fc6Adt2 ($k_0 \approx 1\ s^{-1}$) could tentatively be assigned to conformationally restricted Fc groups, rigidly positioned at a relatively close distance from the surface by peptide chains linked to the gold substrate by the two Adt residues. The similarity between the electronic coupling factors of the two current decay components suggests that also in this case the electron transfer process takes place via electron hopping through the amide sites of the peptide chain.

3.3.3 Square wave voltammetry (SWV)

The CV and CA results reported above strongly suggest that the ET processes under investigation are strongly affected by the dynamical properties of the peptide systems. To further characterize the kinetics of the ET process through the peptide film, SQW measurements were carried out in the 0.3–0.9 V potential range and 8–2000 Hz frequency range using a gold electrode modified by chemisorption of an Fc6Adt2 or an Fc6Adt1 peptide layer. In Figure 8, the electronic current intensities normalized by the pulse frequency as a function of the inverse of the pulse frequency for both the peptide-modified electrodes are reported. The SWV curves revealed a peculiar behavior of the two electro-active peptides, showing for both compounds a similar fast decay at high frequency ($\nu > 200$ Hz) and intensity/frequency peaks centered at 90 Hz (Fc6Adt2) and 40 Hz (Fc6Adt1), respectively.

Some important differences between the two peptides can be observed: i) the intensity/frequency band peaked at 40 Hz for Fc6Adt1 appears significantly broader than that measured in the case of the Fc6Adt2 layer, most likely because of the larger configurational heterogeneity of the former peptide, and ii) a slow increase of the intensity/frequency values at low frequencies can be detected only for Fc6Adt2. This finding parallels the CA results which show an additional slow ET kinetic contribution only for this compound.

It is well known that ET processes in biomolecules or in polymeric systems could be heavily affected by dynamical effects such as backbone contraction or elongation, bending, and conversion between different types of helices. In

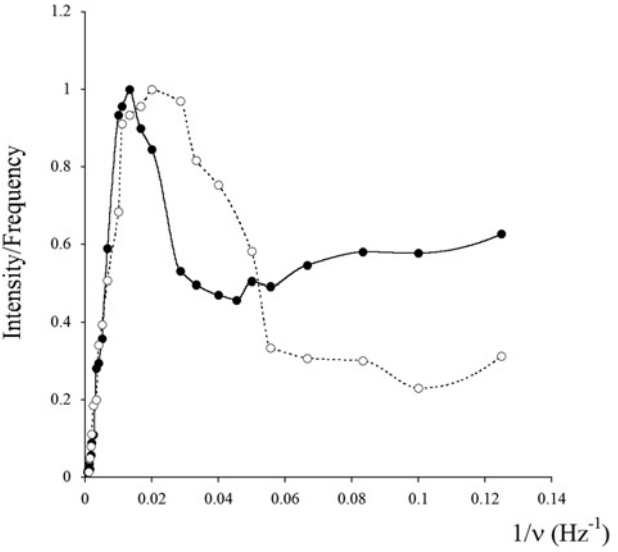

Figure 8: Current intensity/frequency vs. the inverse of the applied SWV pulse frequency. Full circles: Fc6Adt2; Empty circles: Fc6Adt1.

such cases, when molecular motions are restricted, also the ET kinetics become slower [45].

The differences between the two peptide systems revealed by pulsed voltammetry experiments, confirm our working hypothesis that assigns the biphasic ET process observed by CA experiments on Fc6Adt2 to two different ET mechanisms: the faster kinetics involving hopping ET through the amide sites of peptide chains linked to the gold surface by a single Adt residue, and the slower rate constant associated to conformationally constrained Fc groups rigidly located in close proximity to the gold surface.

4 Conclusions

This contribution aims at presenting a new strategy for the functionalization of a gold substrate with a peptide layer through multidentate Au···S interaction. This result was achieved by inserting one or two 4-amino-1,2-dithiolane-4-carboxylic acid (Adt) residues in appropriate positions to realize a single or multiple bidentate linkage of the peptide chain to the gold surface. A stable helical conformation for the two studied hexapeptides was attained by the insertion of four conformationally constrained C^{α}-tetrasubstituted residues (3 Aib and 1 Adt in Fc6Adt1, 2 Aib and 2 Adt in Fc6Adt2) in the peptide chain. Spectroscopic (FTIR,

NMR, ECD) experiments and theoretical conformational analysis confirmed the helical structure of the two peptides.

The binding of the peptide chains and the morphology of the peptide layer on the surface were characterized by XPS and STM experiments, respectively. These techniques revealed some heterogeneity of the peptide layers on gold, mainly caused by the presence of peptide domains formed by peptide chains linked to the surface by two or one Adt residues. As a result, some domains are horizontally layered on the surface showing sub-nanometric heights, while others protrude by 1–2 nm from the surface.

We envisage that a main application of this new approach could be to make it possible an accurate positioning of electro- or optically active probes in the proximity of a gold surface. We proved this issue by analyzing the electrochemical properties of the Fc group functionalizing the peptide chain at its N-terminus.

In particular, CA and SQW measurements confirmed the electroactivity of the Fc probe immobilized on the gold surface, and highlighted the structural and dynamical factors determining the heterogeneity of the electron transfer process.

Recently, we demonstrated that the key factor determining the overall ET efficiency in peptide-based SAMs covalently linked to gold substrates through Au-S interaction is the activated crossing of the electron through the Au$\cdots$S interface (junction effect) [46].

This effect may account for the differences found between peptide chains linked to the gold surface by two or a single Adt residue (the latter is the only possibility for Fc6Adt1). The different linkage to the surface also determines a different topology of the peptide layer on the surface (horizontally or almost vertically arranged with respect to the gold surface) and a different local geometry of the Au$\cdots$S junction. The results reported here clearly show that the ET efficiency is definitely higher for vertically arranged peptide chains, in agreement with the large body of literature that described ET through peptide SAMs in the last decade [47–49].

However, we demonstrated that multiple Au$\cdots$S linkages obtained by inserting multiple Adt residues in the peptide sequence allow for a precise positioning of an electro-active probe in the proximity of a gold surface. Now, back to the title of this contribution, are two Adt residues better than one?

"Not always" is the answer: the choice depends on the application one is planning, preferring to maximize the ET efficiency or the exact positioning of the probe in the proximity of a gold surface. This is an obvious, but not trivial, conclusion. In any case, our view is that Adt does represent a useful tool enriching the peptide materials chemistry kit.

Acknowledgement: This work was supported by the Italian Ministry of Education, University and Research (MIUR), PRIN 2010–2011 No. 2010FM738P, 'Photophysical and photochemical properties of organic and biological compounds in solution and in organized systems'.

References

1. J. C. Love, L. A. Estroff, J. K. Kriebel, R. G. Nuzzo, and G. M. Whitesides, Chem. Rev. **105** (2005) 1103.
2. N. K. Chaki and K. Vijayamohanan, Biosens. Bioelectron. **17** (2002) 1.
3. S. Rana, A. Bajaj, R. Mout, and V. M. Rotello, Adv. Drug Deliver. Rev. **64** (2012) 200.
4. S. Chen, J. Zheng, L. Li, and S. Jiang, J. Am. Chem. Soc. **127** (2005) 14473.
5. M. Halik and A. Hirsch, Adv. Mater. **23** (2011) 2689.
6. E. Gatto and M. Venanzi, Polym. J. **45** (2013) 468.
7. E. Delamarche, B. Michel, H. Kang, and C. Berger, Langmuir **10** (1994) 4103.
8. P. Chinwangso, A. C. Jamison, and T. Randall Lee, Acc. Chem. Res. **44** (2011) 511.
9. C. H. Kim, S. W. Han, T. H. Ha, and K. Kim, Langmuir **15** (1999) 8399.
10. F. Li, L. Tang, W. Zhou, and W. Guo, J. Am. Chem. Soc. **132** (2010) 13059.
11. F. Li, L. Tang, W. Zhou, and W. Guo, Langmuir **26** (2010) 9484.
12. X. Torrelles, C. Vericat, M. E. Vela, M. H. Fonticelli, M. A. Daza Millone, R. Felici, T.-L. Lee, J. Zegenhagen, G. Munoz, J. A. Martin-Gago, and R. C. Salvarezza, J. Phys. Chem. B **110** (2006) 5586.
13. R. Mazzarello, A. Cossaro, A. Verdini, R. Rousseau, L. Casalis, M. F. Danisman, L. Floreano, S. Scandolo, A. Morgante, and G. Scoles, Phys. Rev. Lett. **98** (2007) No. 016102.
14. A. Cossaro, R. Mazzarello, R. Rousseau, L. Casalis, A. Verdini, A. Kohlmeyer, L. Floreano, S. Scandolo, A. Morgante, M. Klein, and G. Scoles, Science **321** (2008) 943.
15. R. G. Nuzzo and D. L. Allara, J. Am. Chem. Soc. **105** (1983) 4481.
16. H. Häkkinen, Nat. Chem. **4** (2012) 443.
17. C. Vericat, M. E. Vela, G. Benitez, P. Carro, and R. C. Salvarezza, Chem. Soc. Rev. **39** (2010) 1805.
18. E. Pensa, E. Cortes, G. Corthey, P. Carro, C. Vericat. M. H. Fonticelli, G. Benitez, A. A. Rubert, and R. C. Salvarezza, Acc. Chem. Res. **45** (2012) 1183.
19. E. Longo, K. Wright, M. Caruso, E. Gatto, A. Palleschi, M. Scarselli, M. De Crescenzi, M. Crisma, F. Formaggio, C. Toniolo, and M. Venanzi, Nanoscale **7** (2015) 15495.
20. T.-Y. Shen and G. L. Walford, Chem. Abs. **75** (1971) 6336j.
21. E. Morera, M. Nalli, F. Pinnen, D. Rossi, and G. Lucente, Bioorg. Med. Chem. Lett. **10** (2000) 1585.
22. D. R. Appleton and B. R. Copp, Tetrahedron Lett. **44** (2003) 8963.
23. F. Formaggio, A. Moretto, M. Crisma, and C. Toniolo, Chemistry of Peptide Materials: Synthetic Aspects and 3D Structural Studies, in: *Peptide Materials. From Nanostructures to Applications*, C. Aleman, A. Bianco, M. Venanzi (Eds.), Wiley, Chichester, UK (2013), p. 39.
24. D. A. Shirley, Phys. Rev. B **5** (1972) 4709.
25. N. L. Allinger, K. Chen, and J.-H. Lii, J. Comput. Chem. **17** (1996) 642.
26. M. Nevins and N. L. Allinger, J. Comput. Chem. **17** (1996) 730.

27. D. F. Kennedy, M. Crisma, C. Toniolo, and D. Chapman, Biochemistry **30** (1991) 6541.
28. B. Pispisa, A. Palleschi, L. Stella, M. Venanzi, C. Mazzuca, F. Formaggio, C. Toniolo, and Q. B. Broxterman, J. Phys. Chem. B **106** (2002) 5733.
29. M. Bellamy, *The Infra-Red Spectra of Complex Molecules*, Methuen, London (1956).
30. F. Formaggio and C. Toniolo, Chirality **22** (2010) E30.
31. A.-S. Duwez, J. Electron Spectrosc. **134** (2004) 97.
32. NIST X-ray Photoelectron Spectroscopy Database, version 2.0 NIST Standard Reference Database 20, US Department of Commerce, Gaitherburg, MD (1997).
33. D. G. Castner, K. Hinds, and D. W. Grainger, Langmuir **12** (1996) 5083.
34. M.-C. Bourg, A. Badia, and R. B. Lennox, J. Phys. Chem. B **104** (2000) 6562.
35. L. H. Dubois, B. R. Zegarski, and R. G. Nuzzo, J. Chem. Phys. **98** (1993) 678.
36. F. Schreiber, A. Ebherardt, T. Y. B. Leung, P. Schwartz, S. M. Wetterer, D. J. Lavrich, L. Berman, O. Fenter, P. Eisenberger, and G. Scoles, Phys. Rev. B **57** (1998) 12476.
37. G. Pace, M. Venanzi, P. Castrucci, M. Scarselli, M. De Crescenzi, A. Palleschi, L. Stella, F. Formaggio, C. Toniolo, and G. Marletta, Mater. Sci. Eng. C **26** (2006) 918.
38. M. A. Brett and A. M. Oliveira Brett, *Electrochemistry. Principles, Methods and Applications*, Oxford Science, Oxford, UK (1993).
39. M. Venanzi, G. Pace, A. Palleschi, L. Stella, P. Castrucci, M. Scarselli, M. De Crescenzi, F. Formaggio, C. Toniolo, and G. Marletta, Surf. Sci. **600** (2006) 409.
40. E. Gatto, L. Stella, F. Formaggio, C. Toniolo, L. Lorenzelli, and M. Venanzi, J. Pept. Sci. **14** (2008) 184.
41. E. Gatto, A. Porchetta, M. Scarselli, M. De Crescenzi, F. Formaggio, C. Toniolo, and M. Venanzi, Langmuir **28** (2012) 2817.
42. E. Katz and I. Willner, Langmuir **13** (1997) 3364.
43. A. L. Eckermann, D. J. Feld, J. A. Shaw, and T. J. Meade, Coordin. Chem. Rev. **254** (2010) 1769.
44. J. Watanabe, T. Morita, and S. Kimura, J. Phys. Chem. B **109** (2005) 14416.
45. A. Anne and C. Demaille, J. Am. Chem. Soc. **128** (2006) 542.
46. E. Gatto, M. Caruso, A. Porchetta, C. Toniolo, F. Formaggio, M. Crisma, and M. Venanzi, J. Pept. Sci. **17** (2011) 124.
47. J. Juhaniewicz, J. Pawlowski, and S. Sek, Isr. J. Chem. **55** (2015) 645.
48. N. Amdurski, ChemPlusChem **80** (2015) 1075.
49. M. Venanzi, E. Gatto, M. Caruso, A. Porchetta, F. Formaggio, and C. Toniolo, J. Phys. Chem. A **118** (2014) 6674.

Supplementary material: 1. Synthesis and characterization of Adt, Fc6Adt1 and their synthetic intermediates; 2. Large scale ($400\,\text{nm} \times 400\text{nm}$) STM images of Fc6Adt1 and Fc6Adt2 on gold. The online version of this article (DOI: 10.1515/zpch-2015-0729) provides supplementary material for authorized users.